# Tag Localization by Handheld UHF RFID Reader and Optical Markers

Aristidis Raptopoulos Chatzistefanou
*School of ECE, AUTH*
Thessaloniki, Greece
raptopak@ece.auth.gr

Antonis G. Dimitriou
*School of ECE, AUTH*
Thessaloniki, Greece
antodimi@auth.gr

***Abstract*—In this paper we design and implement a low-cost mobile handheld human operated device used to locate RFID tags at unknown positions. The device is equipped with a UHF RFID reader, one antenna and a camera. The camera captures and identifies optical markers at known positions, used as landmarks for the accurate 3D estimation of the device's trajectory. This is accomplished by applying Kalman filtering on the on the sequence of captured images. Concurrently, phase measurements from tags at unknown positions are collected, unwrapped and then processed to acquire the 3D locations of the RFID-tagged items. The proposed device is the first to accomplish accurate 3D localization of RFID-tags by a human operated handheld RFID reader. Experimental results reveal mean 3D error in the order of 0.38m.**

***Index Terms*—RFID, handheld, phase, localization, optical markers.**

## I. Introduction

Radio Frequency Identification (RFID) technology has penetrated health care, security market, and assisted living in the last decade. But its most important resides in the field of logistics and particularly inventorying. In the past few years, there has been extensive research in adding accurate localization in the process; a property which has been accomplished successfully by autonomous robots [2]- [8]. In such applications, the authors exploit the precise knowledge of the robot's pose (position and direction) over time, derived by the exploitation of the lidar sensor, typically installed on such robots.

However, such solutions are adopted in large setups (warehouses or retail stores), where retailers can afford the corresponding cost. In smaller stores, retailers are constrained to low-cost handheld RFID readers, which provide only identification (i.e. existence) of a product and not its position. To the best of our knowledge, this is the first paper to accurately address this problem; i.e. inventorying and accurate real-time localization of all products with a handheld RFID device.

In this paper, we propose and construct a handheld UHF RFID reader in order to perform localization of tags by leveraging unwrapped phase of arrival (POA) measurements and optical markers in known positions. We aim to improve and evolve the handheld device presented in [1].

This research has been co-financed by the European Union and Greek national funds through the Operational Program Competitiveness, Entrepreneurship and Innovation, under the call RESEARCH – CREATE – INNOVATE (project code:T2EDK-02000).

Inventorying is usually performed by robots, since it can be automated and unsupervised. In [2] and [3], odometry data and reference RFID tags are used to perform simultaneous localization and mapping (SLAM) and at the same time locate tags in the environment. In [4] and [5], the same means are used to locate the robot in low density reference tag environment. A single passive tag is used in [6]. In [7], the robot exploits odometry sensors and a light detection and ranging (LIDAR) sensor to calculate the trajectory of the antennas it carries. In [8], computer vision assisted position estimation is performed. The trajectory of two antennas is calculated, and their measurements are used to locate tags in the environment.

RFID commercially available off-the-shelf (COTS) devices can measure phase (POA) and power (received signal strength indicator - RSSI). RSSI is highly ambiguous, and most algorithms rely on phase measurements [7], [9], [10]. However, recent works achieve great accuracy by using both measured quantities [11].

In section II, the proposed method is presented. In section III, we describe the conducted experiments, and show the corresponding localization results. Finally, in section IV, conclusions and future work are discussed.

## II. Proposed Method

The proposed method exploits measurements collected by a mobile handheld device, consisting of:

- A UHF RFID reader.
- An optical camera.

The data collected by the camera are used to estimate the camera's pose relatively to a global coordinate system. This is achieved by leveraging optical ArUco markers [12] placed at known poses. At the same time, the RFID reader collects POA measurements from tags at unknown locations. The calculated trajectory of the device is combined with the phase measurements to apply a SAR-based method in order to estimate the positions of the tags in the environment.

### A. Optical Antenna Trajectory Estimation

In this section, we describe how the frames collected by the camera are used to estimate the camera's pose. We used OpenCV [13] to apply the required computer vision algorithms.

Initially, we define the ArUco marker reference system. The $i$-th marker's center is $\mathbf{P}_{mi} = [X_{mi}, Y_{mi}, Z_{mi}]$ in the global coordinate system. Its orientation is defined by a local orthonormal coordinate system $[\hat{\mathbf{x}}_{mi}, \hat{\mathbf{y}}_{mi}, \hat{\mathbf{z}}_{mi}]$, so we need to express these vectors as linear combinations of the global coordinate system orthonormal basis $\left[\hat{\mathbf{x}}_g, \hat{\mathbf{y}}_g, \hat{\mathbf{z}}_g\right]$. An illustration of the above is shown in Fig. 1. For each frame $frame_n$ that the $i$-th frame is visible, we can calculate the rotation vector $\mathbf{rot}_n^i$ and translation vector $\mathbf{tr}_n^i$. These vectors can be explained as follows: if the camera is translated according to $\mathbf{tr}_n^i$, and then rotated according to $\mathbf{rot}_n^i$, it will be aligned with the $i$-th marker. By reversing that process, since the pose of the $i$-th marker is known, we can calculate the position of the camera.

An illustration of the process described in this section is shown in Fig. 2, and it can be broken down to the following steps:

- The camera detects a marker.
- The position of the camera is calculated relatively to the marker.
- Since the pose of the marker is known, the position of the camera in the global coordinate system can be calculated.

At the end of this process, we get the estimations of the camera's position $\mathbf{Pg}_n^i$ calculated based on the detected $i$-th marker at time $t_n^f$.

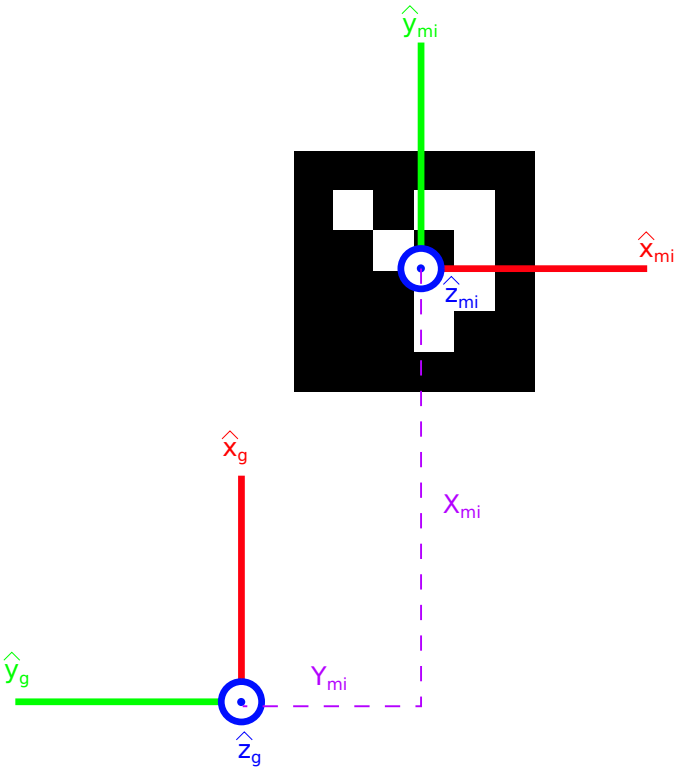


Fig. 1. An example of the local ArUco-centered and global coordinate system relation, as explained in section II-A. The basis $[\hat{\mathbf{x}}_{mi}, \hat{\mathbf{y}}_{mi}, \hat{\mathbf{z}}_{mi}]$ is rotated and translated compared to the global basis $\left[\hat{\mathbf{x}}_g, \hat{\mathbf{y}}_g, \hat{\mathbf{y}}_g\right]$. The rotated local basis vectors can be expressed as linear combinations of the global basis vectors: $\hat{\mathbf{x}}_{mi} = -\hat{\mathbf{y}}_g$, $\hat{\mathbf{y}}_{mi} = \hat{\mathbf{x}}_g$, and $\hat{\mathbf{z}}_{mi} = \hat{\mathbf{z}}_g$. As for the translation, the $X_{mi}$ and $Y_{mi}$ coordinates of the ArUco center are marked with purple.

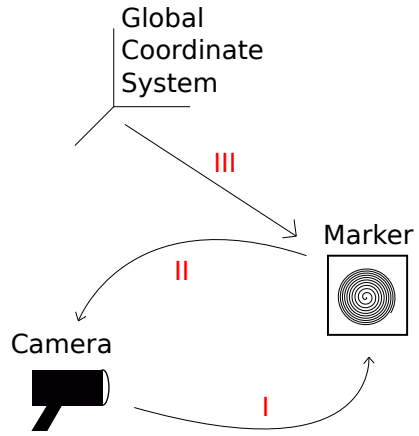


Fig. 2. An illustration of the process described in this section II-A: (I) The camera detects a marker. (II) The relative position of the camera is calculated relatively to the marker. (III) Since the pose of the marker is known, the position of the camera in the global coordinate system can be calculated.

### B. Optical Position Estimation Filtering

In this section, we describe how position estimations we get from the process of section II-A are discarded, if some conditions are not met, and how the remaining estimations are used to get the final position estimation based on the camera data.

Captured frames of low quality may lead to position estimations with great errors. In order to keep our final estimation unaffected by such errors, each estimation $\mathbf{Pg}_n^i$ is discarded, unless it meets the following quality conditions:

- Position estimation $\mathbf{Pg}_n^i$ must be in front of the corresponding $i$-th marker, since the marker is visible from one side only.
- The distance from $\mathbf{Pg}_n^i$ to the $i$-th marker's center must be greater than $R_{min}$ and less than $R_{max}$. If the camera was either too close, or too far from the marker, the position estimation would not be accurate due to the quality of the captured frame.
- The marker must be detected only when seen from a limited angular range $ang_{max}$. As the angle between the camera's facing direction and the marker's $\hat{\mathbf{z}}_{mi}$ vector increases, the area occupied by the marker's depiction on the captured frame decreases, which increases the measurement's ambiguity.

Having discarded $\mathbf{Pg}_n^i$ estimations that do not fulfill the aforementioned conditions, we get the remaining *filtered* estimations $\mathbf{Pf}_n^i$. To continue the filtering process, we group those estimations using overlapping time windows. The estimations of each group are clustered using a k-means clustering algorithm, and the center of the most populated cluster is considered the *windowed* position estimation $\mathbf{Pw}_j$, where $j$ indicates the corresponding time window.

### C. Kalman Filter Application

In this section, we present the Kalman filtering process applied to the position estimations $\mathbf{Pw}_j$. The state that we aim to estimate is the 3D position and velocity $\mathbf{s}_k$ of the antenna:

$$\mathbf{s}_k = [sx_k, sy_k, sz_k, su_{xk}, su_{yk}, su_{zk}]^T \quad (1)$$

The state estimation $\hat{\mathbf{s}}_k$ is calculated by the following equations:

$$K_k = P_k^- H^T \left(R + HP_k^- H^T\right)^{-1} \quad (2)$$

$$\hat{\mathbf{s}}_k = F\hat{\mathbf{s}}_{k-1} + K_k \left(z_k - HF\hat{\mathbf{s}}_{k-1}\right) \quad (3)$$

$$V_j = \left(I - K_k H\right) P_{k-1} \quad (4)$$

$$P_k = FV_k F^T + Q \quad (5)$$

$I$ is the identity matrix. $Q$ and $R$ are noise related parameters of the filter. $F$ is the state transition matrix, and $H$ is the measurement matrix:

$$F = \begin{bmatrix} I_3 & dtI_3 \\ 0_{3\times3} & I_3 \end{bmatrix} \quad (6)$$

$$H = \begin{bmatrix} I_3 & 0_{3\times3} \end{bmatrix} \quad (7)$$

The resulted estimations $\hat{\mathbf{s}}_k$ are then used as the input of a Rauch-Tung-Striebel smoother [14]. The estimations in reverse order are passed through the following process:

$$C_k = V_k F^T P_k^{-1} \quad (8)$$

$$\mathbf{s}_k^* = \hat{\mathbf{s}}_k + C_k \left(\mathbf{s}_{k+1}^* - F\hat{\mathbf{s}}_k\right) \quad (9)$$

$\mathbf{s}_k^*$ are the smoothed state estimations. Let the corresponding position estimations be $\mathbf{PK}_j$. An illustration of the camera trajectory estimation as described in II-A, II-B and II-C is shown in Fig. 3.

### *D. Tag Localization*

In this section, the tag localization is presented. Tags at unknown positions co-exist in the same environment with the optical markers. We use the previously calculated trajectory of the antenna to estimate the positions of the tags.

Localization is achieved according to [9]. Phase measurements from each tag wrapped in $[0, \pi)$ are collected. High read-rate enables phase *unwrapping*. Regarding only one tag, let the unwrapped phase measurement at time $t_j$ be $\phi\left(t_j\right)$. The 3D position $\mathbf{P}_{tag} = [x_{tag}, y_{tag}, z_{tag}]$ of the tag is estimated by solving the following minimization problem:

$$\mathbf{P}_{tag} = \arg\min_{\mathbf{P},c} \sum_j g_{cost}^2(\mathbf{P}, c, j) \quad (10)$$

$$g_{cost}(\mathbf{P}, c, j) = \frac{4\pi}{\lambda} |(\mathbf{PK}_j \mathbf{P})| - \phi\left(t_j\right) + c \quad (11)$$

$\lambda$ is the operating wavelength of the RFID reader. Equation (11) is the difference between the theoretical and measured phase. Equation (10) shows that the estimated position is the one that minimizes the sum of the squares of that difference for all the measurements.

## III. Experimental Results

In this section, experimental results of the proposed method are presented. Optical markers and RFID tags were placed on shelves ($1.4m$ x $1.2m$) in a lab of the School of Electrical and Computer Engineering of Aristotle University of Thessaloniki, as shown in Fig. 4. Optical markers were placed on faces of shelves, and on top of them RFID-tagged items. In total six (6) optical markers were used along with thirty-six (36) tags to be localized. An illustration of the localization results is shown in Fig. 5. The mean of the 3D localization error is 0.38m and its standard deviation 0.25m.

## IV. Conclusions and Future Work

In this paper, we presented a novel method for RFID tag localization using a handheld device. The device first estimates its 3D trajectory using a camera and optical markers in known positions in the environment, and then combines the trajectory estimation with unwrapped phase measurements to localize tags at unknown positions. A prototype of the proposed device was constructed and experimentally tested. The achieved 3D localization error was 0.38m. Future work will be focused on improving the device trajectory estimation and performing more experiments to verify its performance.

## References


[1] A. R. Chatzistefanou, A. Tzitzis, S. Megalou, G. Sergiadis and A. G. Dimitriou, "Target Localization by Mobile Handheld UHF RFID Reader and IMU," in IEEE Journal of Radio Frequency Identification, doi: 10.1109/JRFID.2022.3147539.

[2] E. DiGiampaolo and F. Martinelli, "A Robotic System for Localization of Passive UHF-RFID Tagged Objects on Shelves," in IEEE Sensors Journal, vol. 18, no. 20, pp. 8558-8568, 15 Oct.15, 2018, doi: 10.1109/JSEN.2018.2865339.

[3] E. DiGiampaolo and F. Martinelli, "Mobile Robot Localization Using the Phase of Passive UHF RFID Signals," in IEEE Transactions on Industrial Electronics, vol. 61, no. 1, pp. 365-376, Jan. 2014, doi: 10.1109/TIE.2013.2248333.

[4] F. Shamsfakhr, A. Motroni, L. Palopoli, A. Buffi, P. Nepa, D. Fontanelli, "Robot localisation using UHF-RFID tags: A kalman smoother approach," in Sensors. 21. 717., 2021, 10.3390/s21030717.

[5] A. Motroni, A. Buffi, P. Nepa and B. Tellini, "Sensor-Fusion and Tracking Method for Indoor Vehicles With Low-Density UHF-RFID Tags," in IEEE Transactions on Instrumentation and Measurement, vol. 70, pp. 1-14, 2021, Art no. 8001314, doi: 10.1109/TIM.2020.3027926.

[6] H. Wu, B. Tao, Z. Gong, Z. Yin and H. Ding, "A Standalone RFID-Based Mobile Robot Navigation Method Using Single Passive Tag," in IEEE Transactions on Automation Science and Engineering, vol. 18, no. 4, pp. 1529-1537, Oct. 2021, doi: 10.1109/TASE.2020.3008187.

[7] A. Tzitzis, A. Malama, V. Drakaki, A. Bletsas, T. Yioultsis and A. G. Dimitriou, "Real-Time, Robot-Based, 3D Localization of RFID Tags, by Transforming Phase Measurements to a Linear Optimization Problem," in IEEE Journal of Radio Frequency Identification, doi: 10.1109/JRFID.2021.3103393.

[8] Z. Wang, M. Xu, N. Ye, F. Xiao, R. Wang and H. Huang, "Computer Vision-Assisted 3D Object Localization via COTS RFID Devices and a Monocular Camera," in IEEE Transactions on Mobile Computing, vol. 20, no. 3, pp. 893-908, 1 March 2021, doi: 10.1109/TMC.2019.2954830.

[9] A. Tzitzis et al., "Real-time 3D localization of RFID-tagged products by ground robots and drones with commercial off-the-shelf RFID equipment: Challenges and Solutions," 2020 IEEE International Conference on RFID (RFID), 2020, pp. 1-8, doi: 10.1109/RFID49298.2020.9244904.

[10] P. Tripicchio et al., "A Synthetic Aperture UHF RFID Localization Method by Phase Unwrapping and Hyperbolic Intersection," in IEEE Transactions on Automation Science and Engineering, vol. 19, no. 2, pp. 933-945, April 2022, doi: 10.1109/TASE.2021.3057433.

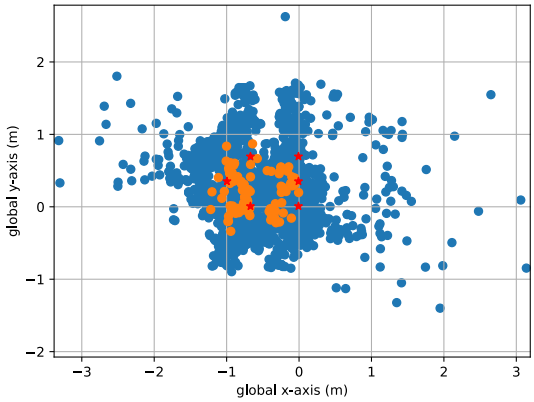


(a) $\mathbf{Pg}_n^i$ (blue) and $\mathbf{Pw}_j$ (orange).

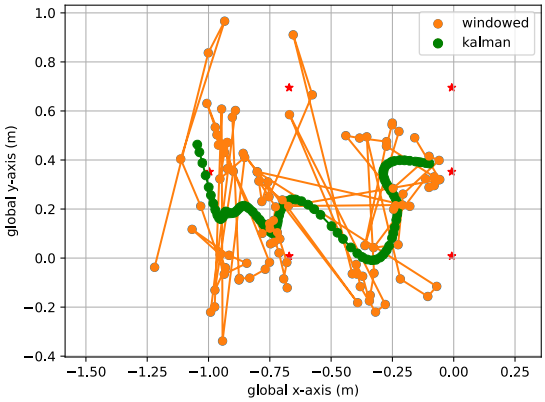


(b) $\mathbf{Pw}_j$ (orange) and $\mathbf{PK}_j$ (green).

Fig. 3. An example of the measurement filtering process described in sections II-A, II-B and II-C. The x-axis and y-axis coordinates are shown in the figures. In the left figure, the blue dots are the original estimations $\mathbf{Pg}_n^i$, and the orange ones the windowed estimations $\mathbf{Pw}_j$. In the right figure, the orange dots are the windowed estimations $\mathbf{Pw}_j$, and the green ones the smoothed estimations $\mathbf{PK}_j$. The red stars represent the positions of the optical markers.

Fig. 4. Photograph of the experiment setup. Optical markers were placed on the faces of some shelves, and on top of them RFID-tagged items. The handheld device was moved in front of the shelves, facing the optical markers.

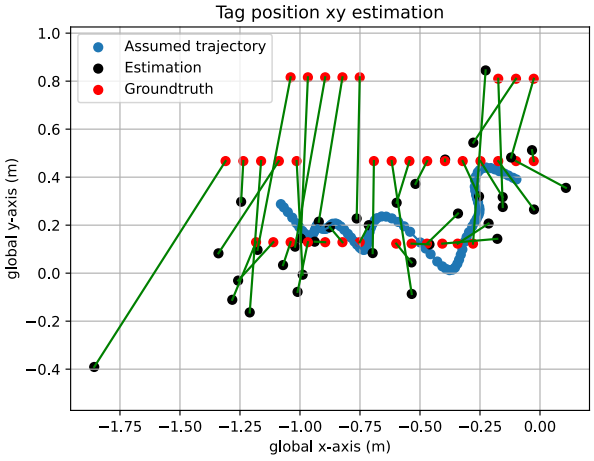


Fig. 5. The tag positions estimations as explained in section II-D. The x-axis and y-axis coordinates are shown in the figures. The red dots represent the groundtruth positions of the tags. Each is connected with a green line to the corresponding estimation shown with a black dot. The assumed antenna trajectory is the blue line.

[11] S. J. Patel and M. J. Zawodniok, "3D Localization of RFID Antenna Tags Using Convolutional Neural Networks," in IEEE Transactions on Instrumentation and Measurement, vol. 71, pp. 1-11, 2022, Art no. 8001311, doi: 10.1109/TIM.2022.3146604.

[12] S. Garrido-Jurado, R. Muñoz-Salinas, F. J. Madrid-Cuevas, and M. J. Marín-Jiménez. 2014. "Automatic generation and detection of highly reliable fiducial markers under occlusion". Pattern Recogn. 47, 6 (June 2014), 2280-2292. DOI=10.1016/j.patcog.2014.01.005

[13] G. Bradski. The OpenCV Library. Dr. Dobb's Journal of Software Tools, 2000.

[14] H. E. Rauch, F. Tung, C. T. Striebel, "Maximum likelihood estimates of linear dynamic systems," in AIAA Journal. 3 (8): 1445–1450, August 1965, doi:10.2514/3.3166.